JGR Oceans

RESEARCH ARTICLE
10.1029/2023JC019774

Wind– and Sea-Ice–Driven Interannual Variability of Antarctic Bottom Water Formation

Christina Schmidt[1,2], **Adele K. Morrison**[3], **and Matthew H. England**[4]

[1]Climate Change Research Centre and Australian Centre for Excellence in Antarctic Science, University of New South Wales, Sydney, NSW, Australia, [2]ARC Centre of Excellence for Climate Extremes, University of New South Wales, Sydney, NSW, Australia, [3]Research School of Earth Sciences and Australian Centre for Excellence in Antarctic Science, Australian National University, Canberra, ACT, Australia, [4]Centre for Marine Science and Innovation (CMSI) and Australian Centre for Excellence in Antarctic Science, University of New South Wales, Sydney, NSW, Australia

Abstract Antarctic Bottom Water (AABW) is a major component of the global overturning circulation, originating around the Antarctic continental margin. In recent decades AABW has both warmed and freshened, but there is also evidence of large interannual variability. The causes of this underlying variability are not yet fully understood, in part due to a lack of ocean and air-sea-ice flux measurements in the region. Here, we simulate the formation and export of AABW from 1958 to 2018 using a global, eddying ocean–sea-ice model in which the four AABW formation regions and transports agree reasonably well with observations. The simulated formation and export of AABW exhibits strong interannual variability which is not correlated between the different formation regions. Reservoirs of very dense waters at depth in the Weddell and Ross Seas following 1–2 years of strong surface water mass transformation can lead to higher AABW export for up to a decade. In Prydz Bay and at the Adélie Coast in contrast, dense water reservoirs do not persist beyond 1 year which we attribute to the narrower shelf extent in the East Antarctic AABW formation regions. The main factor controlling years of high AABW formation are weaker easterly winds, which reduce sea ice import into the AABW formation region, leaving increased areas of open water primed for air-sea buoyancy loss and convective overturning. Our study highlights the variability of simulated AABW formation in all four formation regions, with potential implications for interpreting trends in observational data using only limited duration and coverage.

Plain Language Summary Antarctic Bottom Water (AABW) originates over the Antarctic shelf when sea ice formation and mixing leave behind very cold, salty and dense waters. One third of the total ocean volume is filled by AABW, the densest water mass in the global ocean. AABW is important for climate as it regulates the global ocean overturning of heat, freshwater, oxygen, carbon and nutrients. Although we know that AABW has been warming in recent decades, there are only very limited observations of the year-to-year variability in AABW formation rates. Here, we use a numerical simulation of the global ocean to quantify how much AABW is formed and exported to depth over the period 1958 to 2018. We found that the AABW formation and export changes strongly from year to year. We attribute this variability to changes in wind and sea ice around Antarctica. In general, more AABW is exported during years when the polar easterly winds are weaker, as this influences the sea ice distribution and sea ice formation in the regions of AABW formation. Our findings help to interpret trends and variations in observational data of AABW where only limited duration and coverage is available.

Key Points:

- Strong interannual variability of modeled Antarctic Bottom Water (AABW) formation and export is identified at the four AABW formation sites
- Reservoirs of dense waters in the Weddell/Ross Sea due to strong water mass transformation can lead to higher AABW export for up to a decade
- Increased AABW formation and export is linked to weaker easterlies, less sea ice import, and more areas of open water and sea ice formation

Supporting Information:

Supporting Information may be found in the online version of this article.

Correspondence to:

C. Schmidt,
christina.schmidt@unsw.edu.au

Citation:

Schmidt, C., Morrison, A. K., & England, M. H. (2023). Wind– and sea-ice–driven interannual variability of Antarctic Bottom Water formation. *Journal of Geophysical Research: Oceans*, *128*, e2023JC019774. https://doi.org/10.1029/2023JC019774

Received 22 FEB 2023
Accepted 14 JUN 2023

Author Contributions:

Conceptualization: Christina Schmidt, Adele K. Morrison, Matthew H. England
Data curation: Christina Schmidt
Formal analysis: Christina Schmidt, Adele K. Morrison, Matthew H. England
Funding acquisition: Adele K. Morrison, Matthew H. England
Investigation: Christina Schmidt
Methodology: Christina Schmidt, Adele K. Morrison, Matthew H. England
Project Administration: Adele K. Morrison, Matthew H. England
Resources: Adele K. Morrison, Matthew H. England

1. Introduction

Antarctic Bottom Water (AABW) is a major component of the ocean's meridional overturning circulation, redistributing heat, salt, carbon, and nutrients globally (Talley, 2013). AABW is the densest water mass in the global ocean, filling about one third of the ocean volume and most of the abyssal ocean (Johnson, 2008). In recent decades, there is evidence that AABW has warmed, freshened, and declined in volume (Purkey et al., 2018), but there is also evidence of large interannual variability. For example, a recovery of AABW properties and transport has been measured in the Weddell Sea (Abrahamsen et al., 2019) and the Ross Sea (Silvano et al., 2020) in the second half of the 2010s. The causes of these interannual–decadal variations remain both poorly constrained by a short and sparse record of measurements, and poorly understood. The goal of this study is to examine the variability and mechanisms of AABW formation and export using a global high-resolution ocean–sea-ice model.

Software: Christina Schmidt, Adele K. Morrison
Supervision: Adele K. Morrison, Matthew H. England
Validation: Christina Schmidt
Visualization: Christina Schmidt
Writing – original draft: Christina Schmidt
Writing – review & editing: Christina Schmidt, Adele K. Morrison, Matthew H. England

Trends in the coastal waters around Antarctica where AABW is formed have previously been linked to changes in sea ice transport (Haumann et al., 2016), land-ice melt (Lago & England, 2019; Li et al., 2023; Moorman et al., 2020), local and remote coastal winds (Spence et al., 2014, 2017), or a combination of these processes modulated by variability in large-scale climate modes (Silvano et al., 2020). Warming and reduced formation of AABW has implications for the global ocean heat budget and sea level rise (Purkey & Johnson, 2013) as well as for the ventilation of the deep ocean (Patara & Böning, 2014) and recirculation of nutrients into the upper ocean (Sarmiento et al., 2004). Despite this importance, our knowledge of the connection between Antarctic shelf processes and the abyssal circulation remains incomplete.

Formation of AABW occurs in four main regions around Antarctica: namely, the Weddell Sea, Prydz Bay (also known as Cape Darnley), Adélie Coast and the Ross Sea (Orsi et al., 1999; Purkey et al., 2018). Here, Dense Shelf Water (DSW), a precursor of AABW, is produced by strong heat loss and brine rejection during sea ice formation in coastal polynyas. These polynyas are areas of open water that form when katabatic winds advect sea ice away from the coast. When the DSW cascades down the continental shelf in narrow plumes, it entrains ambient waters to form AABW. In addition, AABW can also be produced by open-ocean deep convection, but this has only been observed on a large scale in the Weddell Sea in the austral winters of 1974–1976 (e.g., Carsey, 1980) and 2017–2018 (e.g., Swart et al., 2018). Guided by topographic features, AABW then spreads northward in the abyss into all major ocean basins (Sen Gupta & England, 2004; Solodoch et al., 2022).

It is challenging to conduct measurements of AABW properties and its formation rate due to the inaccessibility of the mostly sea ice covered formation sites in winter, alongside the small spatial and temporal scales of density-driven convection. Observational data sets on the Antarctic continental shelf and slope are mainly limited to repeated hydrographic sections mostly in summer (e.g., Castagno et al., 2019; Jullion et al., 2013), measurements from mooring arrays with high temporal resolution for single years (e.g., Bowen et al., 2021; Ohshima et al., 2013) or a few moorings in the same position for two decades, for example, in the central Weddell Sea (Gordon et al., 2010, 2020). In the last 10 years, the first deep Argo floats were deployed around Antarctica (Foppert et al., 2021; Kobayashi, 2018) which can measure year-round, cover a larger area than a single mooring, including ice covered regions, and also reach the seafloor. These programs have advanced our knowledge of AABW pathways and properties and will be a valuable tool in the future. However, only a few years of data are currently available, and only in a few isolated regions, with the vast majority of the circumpolar ocean not measured adequately to date. To understand longer-term variations in AABW formation and export, concentrations of chemical tracers like chlorofluorocarbons in AABW can be useful for a circumpolar view (Orsi et al., 1999; Purkey et al., 2018), but again lack high temporal resolution. The only estimate of AABW formation that includes all sources around Antarctica yields a transport off the shelf of 8.1 ± 2.6 Sv (1 Sv = 10^6 m^3 s^{-1}; Orsi et al., 1999, 2002), but the entrainment rate may have been underestimated in these studies (Akhoudas et al., 2021). More studies have investigated the northward flow of AABW as the abyssal limb of the meridional overturning circulation at different latitudes in the Southern Hemisphere, with observational-based estimates at 30°S ranging from 15 to 30 Sv (e.g., Lumpkin & Speer, 2007; Naveira Garabato et al., 2014; Talley, 2013).

The Weddell Sea has traditionally been considered the region with the highest AABW production, with observed estimates of DSW formation using tracer based methods ranging from 3.4 to 4.9 Sv (Akhoudas et al., 2021; Meredith et al., 2001; Orsi et al., 1999). The export of AABW from the Weddell Sea increases to 8–9.7 Sv (Akhoudas et al., 2021; Jullion et al., 2014; Naveira Garabato et al., 2002, 2016) due to the entrainment of Circumpolar Deep Water and DSW flowing in from upstream. The Ross Sea has also long been known as a formation site for AABW (Gordon, 1966; Jacobs et al., 1970). The mean production rate of Ross Sea DSW was estimated to be 1.95 ± 1.85 Sv in 2003 (Whitworth & Orsi, 2006) and ≈1.7 Sv in March 2004 (Gordon et al., 2009). More recently, two other formation sites for AABW have also been discovered. In Prydz Bay, Ohshima et al. (2013) estimated an export of DSW through Wild Canyon of 0.3–0.7 Sv in 2008. Along the Adélie Coast, the annual mean production of AABW was estimated to be 0.4–2.0 Sv during 1998–1999 (Williams et al., 2008).

In addition to overall uncertainty regarding the mean rate of AABW production, there is also a lack of knowledge about its variability. Evidence of interannual variability can, however, be seen in recent measurements; for example, it was shown that the salinity of AABW in the Ross Sea varies strongly (e.g., 0.028 ± 0.003 g kg^{-1} saltier in 2018 compared to 2011) superimposed on a long term freshening trend (Jacobs et al., 2022; Silvano et al., 2020). A rebound in bottom water volume also occurred in the Weddell Sea in 2014–2018 after decades of volume decline (Abrahamsen et al., 2019). Variability in AABW production has been linked to the effect

of winds on sea ice advection and formation in the Weddell and Ross Seas, with either the zonal winds affecting the sea ice advection into the DSW formation region (Silvano et al., 2020) or the meridional winds altering the sea ice transport out of the DSW formation region (Dinniman et al., 2018; McKee et al., 2011; Timmermann, 2002). However, short measurement records have prevented the analysis of interannual–decadal variations.

To overcome these temporal and spatial limitations in the measurement record, numerical models can be used to estimate the mean formation rate of AABW, and its variability, if suitably forced by historical atmospheric fields. Unfortunately, most global ocean and climate models are not able to simulate the processes of AABW formation correctly (Heuzé, 2021; Mensah et al., 2021), and there are considerable biases in hydrographic properties over the shelf (Purich & England, 2021). Often simulated AABW is not sourced from overflowing DSW as the mixing with ambient waters is too strong and instead AABW is produced via open-ocean convection in models. This affects not only the thermohaline properties of the AABW, but also the strength of the lower limb of the meridional overturning circulation. In contrast, the ocean–sea-ice model used in this study has been shown to produce DSW reasonably accurately in the four main formation regions known from observations, from where it flows down the continental shelf into the abyss as AABW (Moorman et al., 2020; Morrison et al., 2020; Solodoch et al., 2022).

Here, we investigate the formation and export of AABW in the four known formation regions from 1958 to 2018 using the global, eddying ocean–sea-ice model ACCESS-OM2-01. We first describe the ocean–sea-ice model in Section 2, alongside the methods used to analyze surface water mass transformation and export of AABW. The simulated interannual variability of AABW formation and export is presented in Section 3, before evaluating the drivers of this variability in Section 4. We conclude the paper with a summary and discussion in Section 5.

2. Model Description and Methods

2.1. The Ocean–Sea-Ice Model ACCESS-OM2-01

The model simulation used in this study is the global ocean–sea-ice model of the Australian Community Climate and Earth System Simulator with a horizontal resolution of 1/10° (ACCESS-OM2-01; Kiss et al., 2020), analyzed over the period 1958–2018. ACCESS-OM2-01 consists of the ocean model MOM (version 5.1; Griffies, 2012) coupled to the sea ice model CICE (version 5.1.2; Hunke et al., 2015), which are forced by 3-hourly atmospheric fields from the JRA55-do data set (version 1.4; Tsujino et al., 2018) from 1958 to 2018 over four consecutive cycles. This modeling strategy follows the OMIP-2 protocol where all cycles except the first one start from the last time step of the modeled ocean state of the previous cycle (Griffies et al., 2016). The analyzed cycle is the third cycle of this simulation which is the only cycle where passive tracers of AABW are also included. Some updates to the ACCESS-OM2-01 model configuration were made, compared to the original version introduced and evaluated by Kiss et al. (2020). These updates are described in detail in Solodoch et al. (2022), where exactly the same simulation years were analyzed, including passive tracers of AABW.

In ACCESS-OM2-01, an Arakawa B-Grid with a global horizontal resolution of 1/10° is used which translates to a zonal and meridional grid spacing on the Antarctic continental shelf of 2.3–5 and 4.7 km, respectively. As the first baroclinic Rossby radius of deformation over the Antarctic continental shelf is between 1.8 and 5.5 km, ACCESS-OM2-01 is not mesoscale resolving at these latitudes, although it is considered eddy-rich in the Antarctic Circumpolar Current, where the Rossby radius is typically 10–20 km. In the vertical, the model has 75 z* levels with partial bottom cells and a layer thickness of 1 m at the surface, increasing to 200 m in the deepest layer and less than 84 m in the upper 1,000 m. Due to a different slope steepness in the AABW formation regions, this horizontal resolution might not be sufficient to simulate the export of AABW everywhere. Using a regional model of Prydz Bay at different resolutions it was shown that the export of AABW is reduced at a horizontal resolution $\geq$2 km due to excessive mixing and transformation of DSW into intermediate waters during the downslope flow (Mensah et al., 2021). A comparable slope steepness in Prydz Bay and along the Adélie Coast suggests a reduced DSW/AABW export in models of 1/10° resolution, whereas this resolution is likely sufficient to simulate the downslope flow of DSW in the Weddell and Ross Seas where the continental slope is not as steep. We analyze the export of AABW across the 1,000-m isobath as most of the spurious mixing is expected in deeper layers, and the aim of this study is to assess the origin of AABW interannual variability, rather than its downstream propagation.

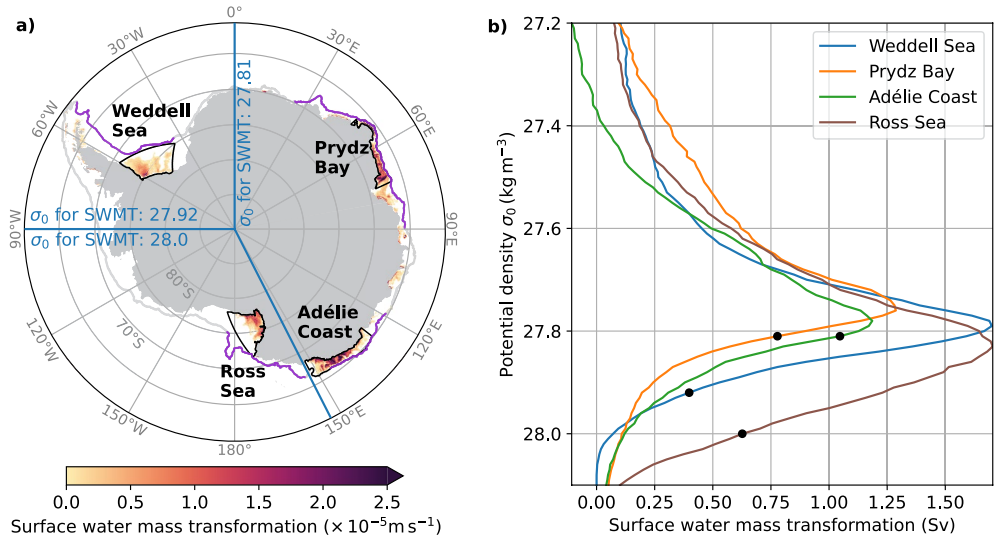

Figure 1. Regions and rates of Dense Shelf Water formation in ACCESS-OM2-01 estimated by the mean (1958–2018) surface water mass transformation (SWMT). (a) The SWMT per unit area across a certain potential density class σ_0 (Weddell Sea: $\sigma_0 = 27.92$ kg m^{-3}, Prydz Bay and the Adélie Coast: $\sigma_0 = 27.81$ kg m^{-3}, and Ross Sea: $\sigma_0 = 28.0$ kg m^{-3}) into downwelling density classes is shown on the continental shelf in red shading. The black contour outlines the area used to integrate the SWMT in each region. The gray line is the 1,000-m isobath and the Antarctic Bottom Water export is calculated across the sections highlighted in purple. (b) SWMT integrated over each of the four regions indicated by the black contours in (a). The circles show the potential density class chosen to calculate the rate of SWMT throughout this study.

ACCESS-OM2-01 lacks ice shelf cavities and tides, both of which affect the properties and export of waters transformed on the shelf (Bowen et al., 2021; Stewart, 2021). In addition, the forcing data set JRA55-do only provides a climatological mean of Antarctic calving and basal melt (based on Depoorter et al. (2013)), so in this study there is no variability in the formation rate of DSW/AABW due to variations and trends in the melting of Antarctic ice sheets. Despite these limitations, ACCESS-OM2-01 is still overall realistic in its representation of the processes and regions of AABW formation (Moorman et al., 2020; Morrison et al., 2020). Adopting a higher resolution model, or a model with more components and complexity, is not presently feasible for a global simulation run over centennial time-scales.

2.2. Surface Water Mass Transformation and Export of AABW

We use the surface water mass transformation (SWMT) analysis following Newsom et al. (2016) and Abernathey et al. (2016) to estimate the rate at which surface waters are transformed into downwelling density classes due to surface buoyancy forcing. The SWMT rate is defined as the volume flux into a particular potential density class due to heat and salt fluxes (see Appendix A for more details). For each region, the SWMT was integrated over the area on the Antarctic shelf indicated by the black contours in Figure 1a where the SWMT (red colors) is most pronounced. As the thermohaline properties of the shelf water vary around Antarctica, the potential density class used for the SWMT calculation differs between formation regions. The potential density class was chosen such that the correlation with AABW export across the 1,000-m isobath (defined below) was highest. The resulting potential density class used (circles in Figure 1b) is lightest off the Adélie Coast and in Prydz Bay ($\sigma_0 = 27.81$ kg m^{-3}), denser in the Weddell Sea ($\sigma_0 = 27.92$ kg m^{-3}) and densest in the Ross Sea ($\sigma_0 = 28.0$ kg m^{-3}). The choice of the potential density class for the calculation of the SWMT mainly affects the mean formation rate, with the variability being overall robust to this choice, so long as the potential density class is below the peak SWMT (Figure A1).

The export of AABW from the continental shelf into the open ocean across the 1,000-m isobath was calculated using daily model output. Furthermore, we made use of passive dye-like tracers, which were released at the surface in the four DSW formation regions (i.e., four separate tracers are used). These passive tracers are set to 1 in each of the four formation locations, and set to 0 at the surface everywhere else to avoid leakage into adjacent DSW formation sites over time (see Solodoch et al. (2022) for more details). First, the transport across the 1,000-m isobath was binned into isopycnal bins. Second, this transport was summed along the isobath adjacent

Table 1
Mean, Standard Deviation (std), and Surface Referenced Density (σ_0) of Surface Water Mass Transformation (SWMT) and Antarctic Bottom Water (AABW) Export for the Four Main Formation Sites

	Mean ± std (Sv)		σ_0 (kg m^{-3})	
Region	SWMT	AABW export	SWMT (σ_0 class)	AABW export (mean σ_0)
Weddell Sea	0.4 ± 0.4	1.5 ± 0.6	27.92	27.84
Prydz Bay	0.8 ± 0.3	2.8 ± 0.3	27.81	27.80
Adélie Coast	1.0 ± 0.4	1.5 ± 0.4	27.81	27.86
Ross Sea	0.6 ± 0.5	2.9 ± 0.6	28.00	27.87
Total	2.9 ± 0.8	8.6 ± 0.9		

Note. Surface referenced density values (σ_0) are shown to indicate the potential density class of SWMT, and the transport-weighted mean potential density of the AABW export (whose density and layer thickness varies in time).

to and downstream of each formation region (purple section of the 1,000-m isobath in Figure 1a), where the mean concentration in 1958–2018 of the locally released passive tracer was at least 15% in the bottom-most grid cell. If a lower passive tracer concentration is used as a threshold, sections of the isobath start to overlap between some regions and the same transport would be considered twice. The variability of the transport is robust for higher thresholds of passive tracer concentration, only the mean transport value reduces. Third, the cumulative sum of the transport in potential density space was calculated from the bottom upwards and its maximum in the vertical was considered to be the total offshore transport of AABW. We refer to this offshore transport of AABW across the 1,000-m isobath as AABW export throughout the study. This definition of AABW export allows the upper potential density threshold and layer thickness to vary temporally on daily, to seasonal and interannual time scales. Due to a pronounced seasonal cycle in some of the formation regions, with a maximum AABW export between spring and autumn depending on the region (Figures 4e–4h), a yearly average was computed starting in austral winter in the month of the minimum AABW export (namely, September in the Weddell Sea, August in Prydz Bay and the Ross Sea, and June at the Adélie Coast).

We can not directly estimate the entrainment rate by comparing the SWMT with the AABW export, due to different densities being used for each of these two metrics. First, the density of the AABW export varies in time. Second, the density classes across which the SWMT is estimated is often higher than the mean density of the AABW export (Table 1) as mixing with lighter waters occurs along the way to the shelf break. Using lighter density classes, which are comparable to the densities of the AABW export, to estimate the SWMT would likely capture water, which after mixing with even lighter waters, is too light to overflow and form AABW.

The mean export of AABW is highest from Prydz Bay and the Ross Sea, each accounting for about a third of the total AABW export, with the Weddell Sea and Adélie Coast each contributing a similar export of the remaining fraction (Table 1). Although the formation and export from the Weddell continental shelf is lower compared to observations, possibly due to the lack of ice shelf cavities in the model, the export of AABW from the other regions is within the range of observational estimates. The mean net AABW export from all four regions is 8.6 ± 0.9 Sv averaged over 1958–2018. Although this agrees well with the estimate of 8.1 ± 2.6 Sv by Orsi et al. (1999, 2002), it has been shown that the entrainment rate in the observational estimate of Orsi et al. (1999, 2002) was likely underestimated (Akhoudas et al., 2021) suggesting that the AABW formation in ACCESS-OM2-01 could be too weak. Further north at 30°S, an abyssal northward flow of 17.6 Sv under the mean depth of the $\sigma_2 = 37.08$ kg m^{-3} isopycnal (Solodoch et al., 2022) is within the range of 15–30 Sv estimated from observations (Lumpkin & Speer, 2007; Naveira Garabato et al., 2014; Talley, 2013). Note finally that the ratio of AABW export across the shelf break from the different regions is not necessarily the same as the ratio of transport exported into the abyss of the Southern Ocean because of varying entrainment in the overflows and exit passages.

2.3. Climate Indices

We also analyze whether the variability in Antarctic shelf SWMT can be linked to climate modes or atmospheric circulation, including the Southern Annular Mode and the Amundsen Sea Low. For this purpose, the Southern Annular Mode index is defined as the difference between the monthly, zonally averaged sea level pressure between 40° and 65°S (after Marshall (2003)). The region between the Ross Sea and the Antarctic Peninsula is influenced by the Amundsen Sea Low (Hosking et al., 2013) whose strength is described by the Amundsen Sea Low index (minimum in monthly sea level pressure between 60°–75°S and 180°–310°E; Turner et al., 2013).

2.4. Statistical Methods

Linear correlations (Pearson correlation) were calculated after linearly detrending all time series. The student's *t*-test was used to define statistically significant correlations indicated by the *p*-value. Auto-correlation was accounted for by considering the effective degrees of freedom via the e-folding time scale.

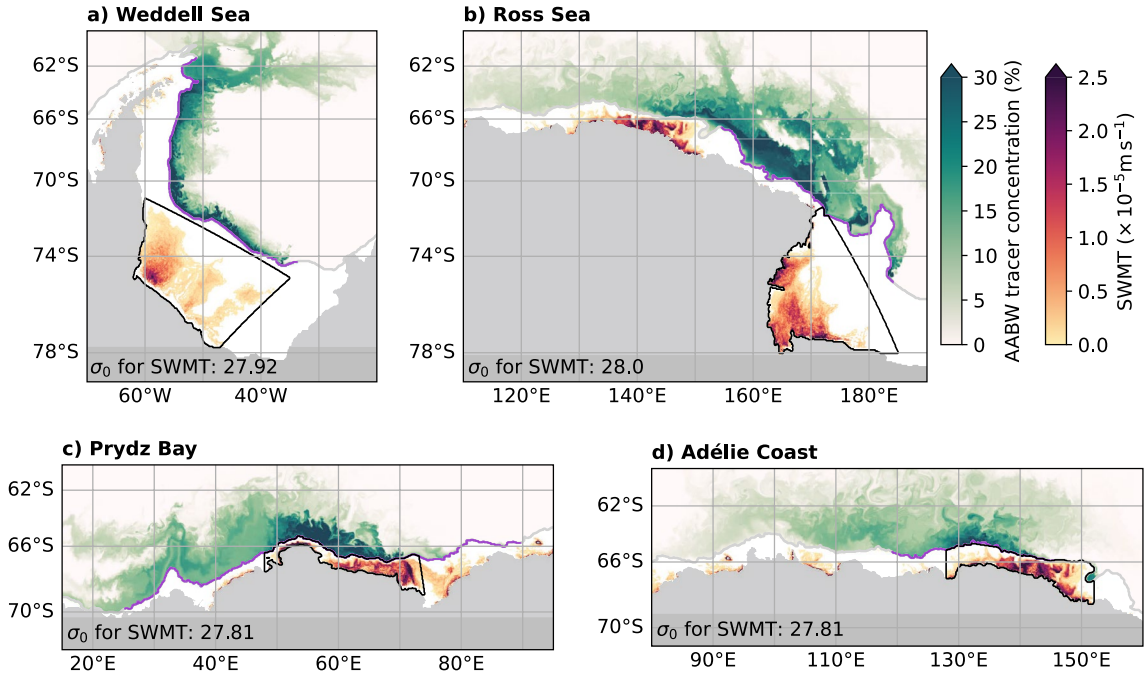

Figure 2. Formation regions of Dense Shelf Water (DSW) and pathways of Antarctic Bottom Water (AABW). The mean (1958–2018) surface water mass transformation (SWMT) per unit area across a certain potential density class σ_0 is shown on the continental shelf in red shading in the (a) Weddell Sea ($\sigma_0 = 27.92$ kg m^{-3}), (b) Ross Sea ($\sigma_0 = 28.0$ kg m^{-3}), (c) Prydz Bay ($\sigma_0 = 27.81$ kg m^{-3}), and (d) Adélie Coast ($\sigma_0 = 27.81$ kg m^{-3}). The black contour outlines the area used to integrate the SWMT in each region. The gray line is the 1,000-m isobath and the AABW export is calculated across the sections highlighted in purple. A snapshot of the AABW tracer concentration in the bottom-most grid cell on 1 January 1962 (i.e., after 4 years of model integration) is shown at depths greater than 1,000-m as green shading, indicating the main DSW/AABW pathways.

3. Variability of DSW Formation and AABW Export

High rates of SWMT on the continental shelf in the Weddell Sea, in Prydz Bay, along the Adélie Coast and in the Ross Sea indicate the formation of DSW (Figures 1a and 2). The export of DSW down the continental slope north and downstream of the formation region and into the abyss as AABW is visible in the passive tracer distribution (Figure 2, green shading). In the Weddell and Ross Seas, the SWMT is especially high on the western continental shelf, but the exact region in which the SWMT occurs is highly variable from year to year in both location and size (Figures 3a–3e, 3j, and 3k). In Prydz Bay and off the Adélie Coast, the strongest SWMT occurs in a similar location each year. The area of the SWMT extends mostly in a zonal sense in these two sectors (Figure 3f–3i) compared to the Ross and Weddell Shelf regions, where the area of SWMT also extends in a meridional sense as the coastal geometry is markedly different. The SWMT exhibits a strong seasonal cycle with a maximum in austral winter (namely, August in the Weddell Sea and Adélie Coast and September in Prydz Bay and the Ross Sea) and no SWMT into downwelling density classes in summer (Figures 4a–4d). The large standard deviation of the SWMT (shading in Figures 4a–4d) indicates not only strong interannual variability of the strength of the SWMT but also variability in the duration and onset of the SWMT. For example, the onset of the SWMT in the Weddell Sea can appear as early as April, but in some years starts as late as October, with the peak in SWMT occurring between August and October in only 67% of the years analyzed. Between 1958 and 2018, the SWMT rate varies strongly on interannual to decadal time scales (Figure 5, black lines). Especially in the Weddell and Ross Seas, the SWMT in the chosen potential density class collapses to near 0 Sv in some years, although surface waters are still transformed into lighter downwelling classes such that DSW is still formed, but with lighter potential densities (Figure A1). In other years, up to 1.5–2 Sv of SWMT occur in each of the four regions of DSW formation.

The variability in the SWMT is reflected in the AABW export, which is defined as the offshore transport of AABW across the 1,000-m isobath north and downstream of the formation regions (Figure 5, purple lines). The AABW export is in general larger than the SWMT due to entrainment, with even more entrainment occurring when the DSW descends off the shelf and into the abyss. A greater distance between the locations of SWMT and

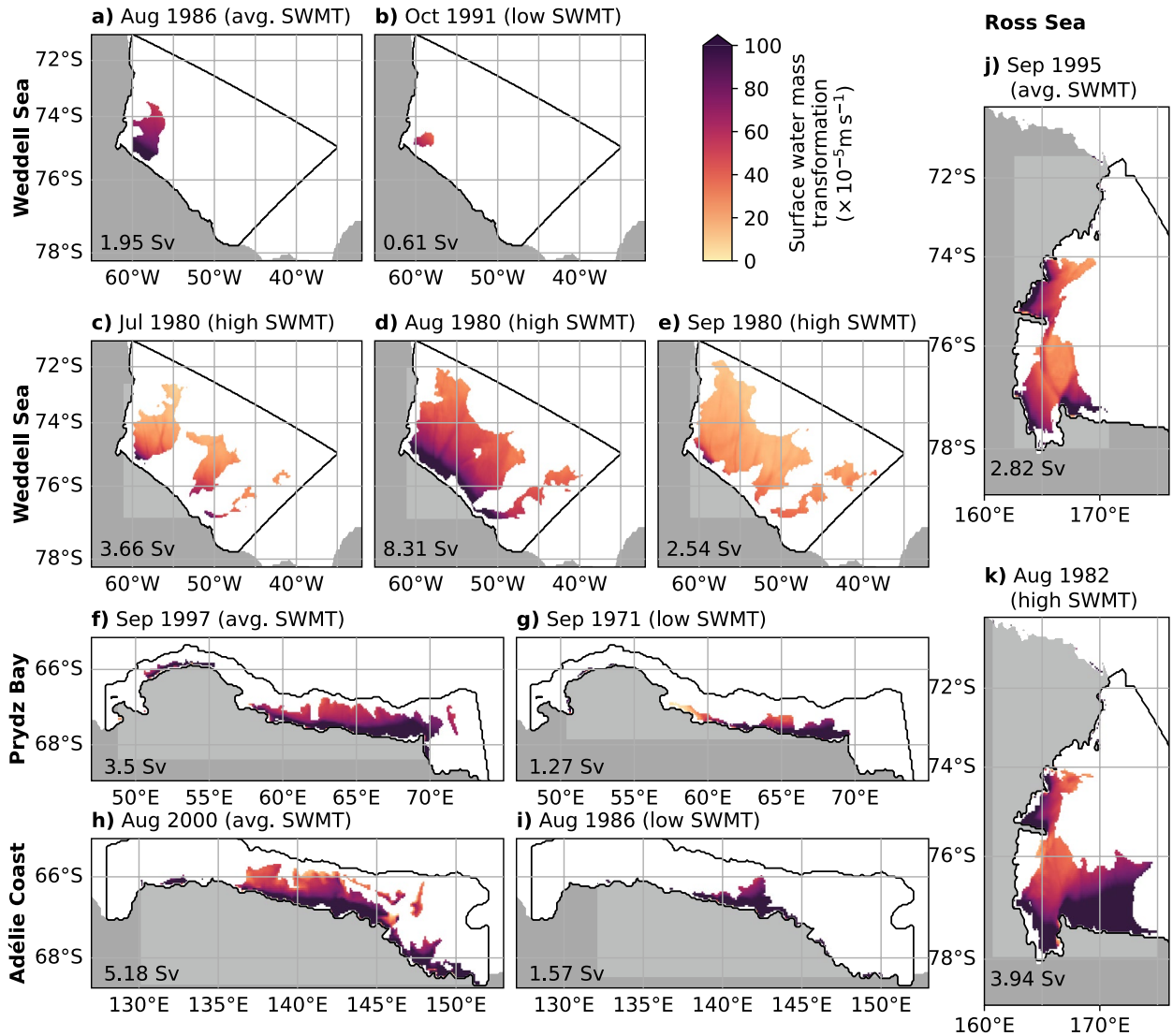

Figure 3. Surface water mass transformation (SWMT) for selected months and years of low, average, or high SWMT, highlighting interannual variations in the region of SWMT in the (a–e) Weddell Sea, (f–g) Prydz Bay, (h–i) Adélie Coast, and (j–k) Ross Sea. (c–e) show the month before, of, and after the peak SWMT in the Weddell Sea in 1980. The monthly mean SWMT in Sv is given in the lower left corner of each panel.

the 1,000-m isobath in the Weddell and Ross Seas compared to Prydz Bay and the Adélie Coast likely results in higher entrainment in the Weddell and Ross Seas and hence increased AABW export. A large difference between the potential density used for the calculation of the SWMT and the mean potential density of AABW export indicates a high entrainment rate. This might explain why the highest increase between the SWMT and AABW export (~2 Sv) is in the Ross Sea, given the large difference in potential densities used for the SWMT (28 kg m^{-3}) and AABW export (27.87 kg m^{-3}) in that sector. Another factor resulting in a higher AABW export relative to SWMT is the advection of DSW from upstream, which explains the majority of the offset compared to the SWMT in Prydz Bay (with on average 1.47 Sv of water with density $\sigma_0 > 27.8$ kg m^{-3} entering Prydz Bay on the shelf from the east, compared to 0.0 Sv exiting to the west).

The interannual variability of AABW export (Figure 5, purple lines) is highest out of the Weddell and Ross Seas, with a standard deviation of 0.6 Sv (Table 1) and dominant time scales in the Weddell Sea of 6 years/cyc and in the Ross Sea between 4 and 5 years/cyc, which are significantly ($p < 0.01$) different from red and white noise. In the two other regions, the variability occurs on shorter time scales of 2–3 years/cyc, but is only significant in Prydz Bay. The link between the SWMT and AABW export on interannual time scales is strongest at the Adélie Coast ($r = 0.92$, $p < 0.01$), but very high correlations of $r = 0.78$ ($p < 0.01$) in the Weddell Sea and $r = 0.89$

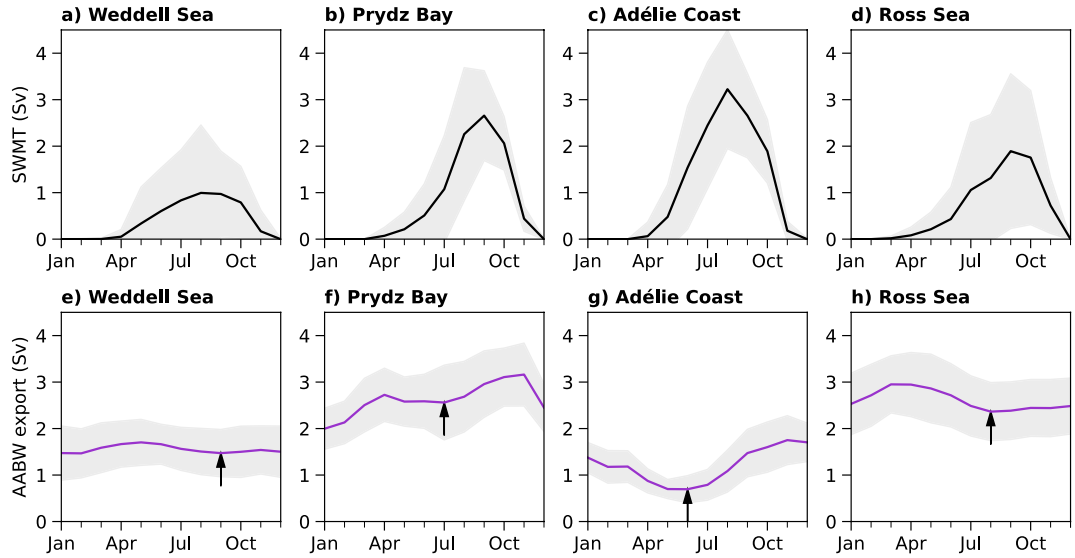

Figure 4. Seasonal cycle of (a–d) surface water mass transformation (SWMT) and (e–h) Antarctic Bottom Water (AABW) export in the (a, e) Weddell Sea, (b, f) Prydz Bay, (c, g) Adélie Coast, and (d, h) Ross Sea. The SWMT is integrated over each of the four regions indicated by the black contour in Figure 2. The AABW export is the transport summed along the 1,000-m isobath downstream of each formation region (purple sections of the 1,000-m isobath in Figure 2). The gray shading shows the standard deviation and the arrows in (e–h) indicate the month of the minimum AABW export in winter.

($p < 0.01$) in the Ross Sea exist as well. There is, however, no significant correlation between the four formation regions in either the SWMT or the AABW export, apart from AABW export exhibiting some co-variability between the Ross Sea and Adélie Coast ($r = -0.42$, $p < 0.01$). These two formation regions are in closest proximity to each other and experience opposite changes in AABW export in the 1970s, with a decline in the Adélie Coast region coinciding with an increase in the Ross Sea. The overall weak correlation between SWMT rates across the four formation regions suggests that the drivers of variability in DSW and AABW production in each sector are due to independent local forcing mechanisms.

In agreement with observations (Pellichero et al., 2018), the SWMT into dense waters is due to salinity fluxes which originate mostly from brine rejection during sea ice formation. Therefore, the majority of the SWMT variability can be attributed to sea ice growth (e.g., as shown for the Ross Sea in Figure A2). Indeed, the correlations between the SWMT and the annual sum of sea ice growth in the area where the SWMT occurs each month is in the range 0.90–0.95 ($p < 0.01$), depending on the region. The sea ice growth integrated over the whole region used to calculate the SWMT (black contours in Figure 2) is however not correlated to the SWMT, which emphasizes the importance of localized sea ice growth for the SWMT and hence formation of DSW.

Salinity variability in the DSW formation regions can be further examined to understand the connection between SWMT and AABW export. For example, subsequent to strong events of SWMT, reservoirs of high salinity water can accumulate at depth, leading to higher AABW export for up to a decade. These reservoirs of very saline DSW at depth are especially visible in the Hovmöller diagram of the spatial mean salinity in the Weddell Sea (averaged over the area within the black contour in Figure 2a) in the 1960s, 1980s, and from the late 1990s to mid 2000s (Figure 6a). Here, the accumulation of saline DSW can be attributed to strong SWMT events in single years (i.e., 1962, 1980, and 1998; see black line in Figure 6b). The 1980s record reveals the best example of this mechanism where the SWMT, the salinity at 0–300 m, and the AABW export are all exceptionally high in 1980 (Figure 6b), and the SWMT in the ensuing years is relatively low. In contrast, both the salinity at 0–300 m and the AABW export remain relatively high over the ensuing 8 years. In this analysis, a depth range in the upper 300 m of the water column was chosen for the time series of the salinity shown in Figure 6 as this lies within the winter mixed layer in all four regions. Similar analyses undertaken over different depth ranges, including the full water column, show robust results to those presented in Figure 6. Furthermore, the mean was calculated from August to October (late winter) as this best reflects the water mass modification during the formation of DSW and results in high correlations with both the SWMT and AABW export (Table 2). This build up of saline and dense waters at depth can also be seen in the Ross Sea (Figure 6c).

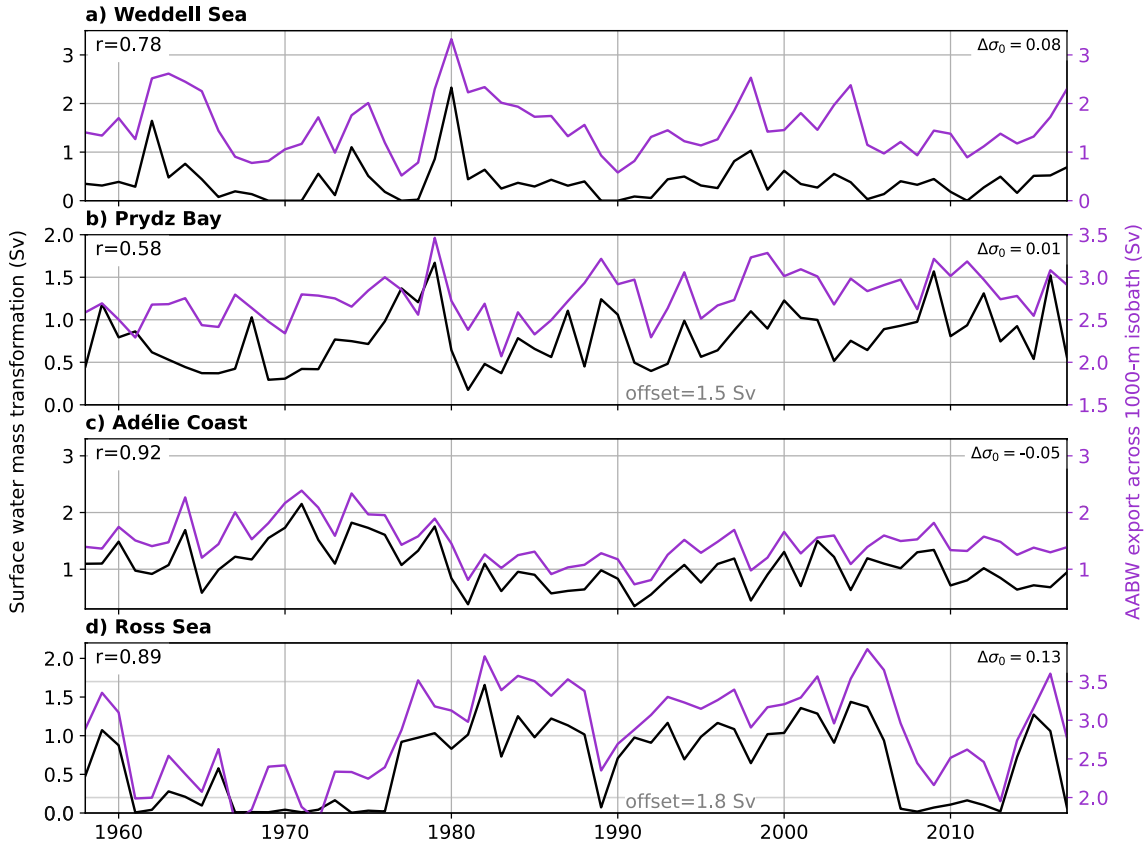

Figure 5. Annual time series of surface water mass transformation (SWMT, black lines) and Antarctic Bottom Water (AABW) export across the 1,000-m isobath (purple lines) in the (a) Weddell Sea, (b) Prydz Bay, (c) Adélie Coast, and (d) Ross Sea. The SWMT is integrated over each of the four regions indicated by the black contour in Figure 2. The AABW export is the transport summed along the 1,000-m isobath downstream of each formation region (purple sections of the 1,000-m isobath in Figure 2). The correlation coefficient r between the SWMT and AABW export is given. $\Delta\sigma_0$ is the potential density of the SWMT minus the average potential density of the AABW export. Note that the y-axis of the AABW export is offset by 1.5 Sv in (b) and 1.8 Sv in (d) but the scale is the same otherwise.

In Prydz Bay and at the Adélie Coast, the seasonal cycle in salinity reaches all through the water column and there is no evidence for pronounced reservoirs of high salinity waters at depth persisting for several years (Figure 7a for Prydz Bay and Figure 7c for the Adélie Coast). We attribute the absence of reservoirs of very saline DSW to a more rapid export of DSW due to the narrower shelf extent in the East Antarctic DSW formation regions, compared to the Weddell and Ross Seas, which are characterized by large embayments with a shelf depth of approximately 300–500 m and 350–700 m, respectively.

4. Drivers of DSW and AABW Variability

Here, we explore the drivers of the simulated AABW formation and export and show that years of high AABW formation and export are often associated with weaker easterly winds, which lead to reduced sea ice import into the DSW formation region and increased areas of open water. We also examined the meridional component of the wind stress, sea ice growth, sea ice concentration, sea ice volume tendency due to dynamics or thermodynamics, area of the SWMT, and salt advection into the DSW region, but did not find significant correlations with the SWMT, salinity in the DSW formation region, and AABW export. A multiple linear regression model of the upstream zonal and offshore meridional wind stress onto the salinity in the DSW formation region improved the correlations only slightly and confirmed the importance of the zonal wind stress. In the following, we focus on the correlations with the mean salinity at 0–300 m in the DSW region between August and October (red lines in Figures 6 and 7), as the salinity is highly correlated with both the SWMT and AABW export (Table 2). Furthermore, the time series of the SWMT only includes transformation into one specific potential density class, and the AABW export across the 1000-m isobath also contains other entrained waters not recently exposed to surface

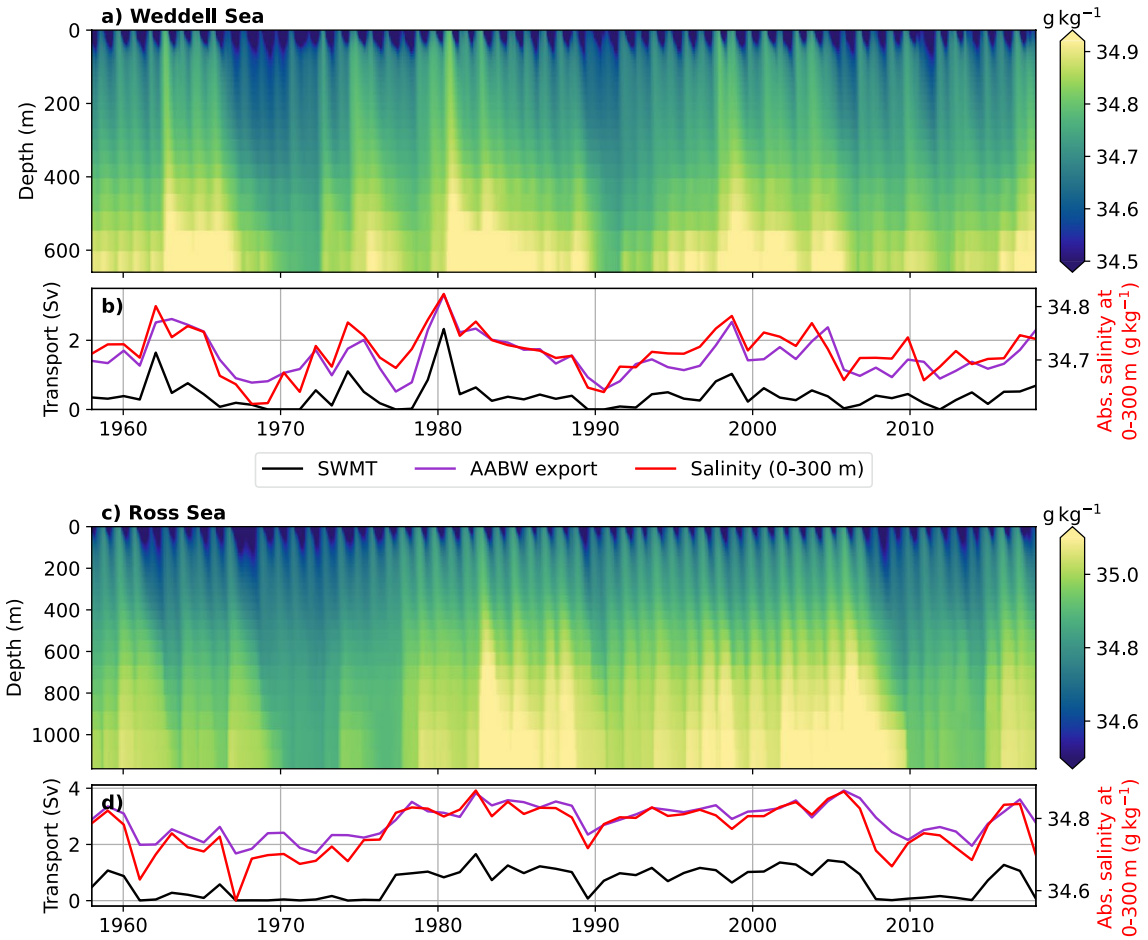

Figure 6. Absolute salinity averaged in the Dense Shelf Water formation region (black contour in Figure 2) in the (a, b) Weddell Sea and (c, d) Ross Sea. (a) and (c) show Hovmöller diagrams of monthly means over the full depth and (b) and (d) show a time series of the salinity averaged in the upper 300 m for August to October (red) together with the SWMT (black) and AABW export (purple) from Figure 5.

forcing. In contrast to these limitations, the salinity at 0–300 m in the DSW region better captures the interannual variability of DSW formation due to surface forcing.

First, we analyze the effect of the variability in zonal wind stress on the salinity in the DSW formation regions. The winds around Antarctica are commonly referred to as "polar easterlies," but due to guidance by the Antarctic continental orography, the surface winds are not purely zonal and more closely follow the coastline. Upstream of the four DSW formation regions, however, the magnitude of the zonal component does generally exceed the meridional component, and the winds are mostly easterlies. Often in years of high salinity in the DSW formation region (and hence high AABW formation and export), the easterlies weaken or even reverse direction (Figure 8). Figures 8a–8d illustrate this positive correlation between the salinity in each DSW formation region and the zonal wind stress at each location (noting that easterly winds are negative in sign). The zonal wind stress was averaged over 6 months between summer and winter for all regions except for Prydz Bay where January–February was used (see Table 3 for months). For these months the correlation with the salinity in the DSW formation region in the following winter is especially high as the preconditioning for the sea ice formation in the following winter occurs, but the months selected vary between regions due to different geographical and atmospheric conditions.

Table 2
Correlation Coefficients Between the Salinity in the Dense Shelf Water Formation Region at 0–300 m for August to October and the Surface Water Mass Transformation (SWMT) and Antarctic Bottom Water (AABW) Export

	SWMT		AABW export	
Region	*r*	Months	*r*	Months
Weddell Sea	0.80	January–December	0.82	September–August
Prydz Bay	0.92	January–December	0.64	August–July
Adélie Coast	0.77	January–December	0.73	June–May
Ross Sea	0.92	January–December	0.90	August–July

Note. All correlations shown are significant at the 99% confidence level. The months used to calculate the temporal means are given for each variable.

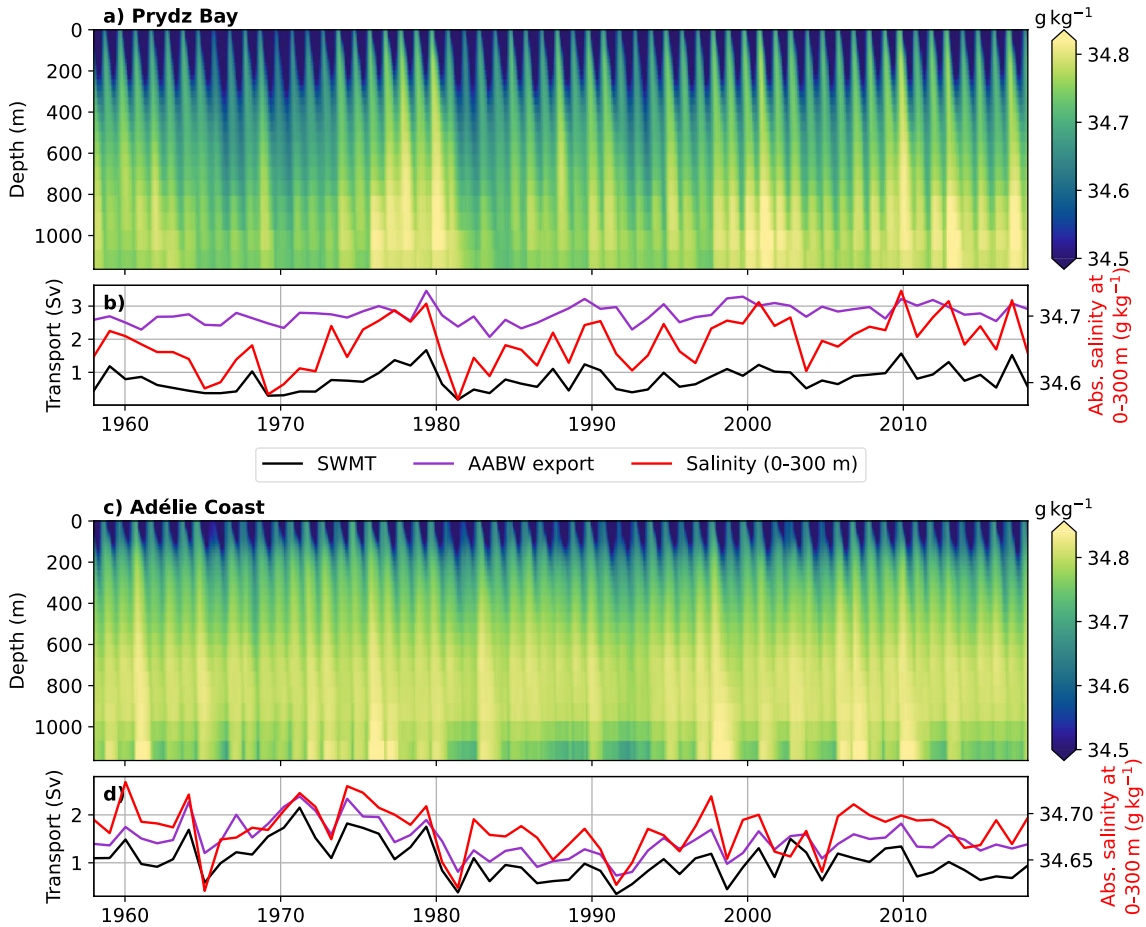

Figure 7. As in Figure 6 but for (a, b) Prydz Bay and (c, d) the Adélie Coast.

For all four regions, the positive correlation prevails over a large sector of the Southern Ocean and is especially high upstream (i.e., eastwards) and offshore of the formation region (indicated by the cyan boxes in Figures 8a–8d). The link between the zonal wind stress averaged over these regions of high correlation and the salinity in the DSW formation region is shown in Figures 8e–8h for all regions. A reversal of the zonal wind from easterlies (negative wind stress) to westerlies is evident in the Weddell Sea ($r = 0.53$, $p < 0.01$), in Prydz Bay ($r = 0.53$, $p < 0.01$), and in the Ross Sea ($r = 0.59$, $p < 0.01$) in years of increased salinity in the DSW formation regions, whereas the easterlies only weaken at the Adélie Coast ($r = 0.55$, $p < 0.01$). In Prydz Bay, the increased zonal winds in January–February are related to the positive phase of the Southern Annular Mode, with a correlation of 0.75 ($p < 0.01$) between the mean zonal wind stress in the cyan box and the Southern Annular Mode index averaged over January and February. Close to the Antarctic continent in the Amundsen and Ross Seas, a weaker Amundsen Sea Low can explain the weaker easterlies only to a small extent, and the variability of the zonal wind stress upstream of the Ross Sea is not significantly correlated to the Amundsen Sea Low index ($r = 0.14$, $p > 0.05$).

One mechanism through which zonal winds affect the AABW formation is via influencing sea ice transport into the DSW formation region. To examine this process, the sea ice transport was calculated across a section east and hence upstream of the DSW formation region that extends 3° from the coast to the north (yellow lines in Figures 8a–8d). The transport is defined as positive into the DSW formation region (i.e., westward) and computed from daily averages of sea ice velocity and sea ice thickness. We correlated the sea ice transport into the DSW formation region with the zonal wind stress upstream of the DSW formation region (averaged over cyan regions in Figure 8, except for Prydz Bay where an average over the blue region in Figure 8b is used as it aligns with the section for the sea ice transport). The temporal mean was calculated for the months matching the months used for the wind stress; namely, January–June except for the Adélie Coast where April–September is used. A negative

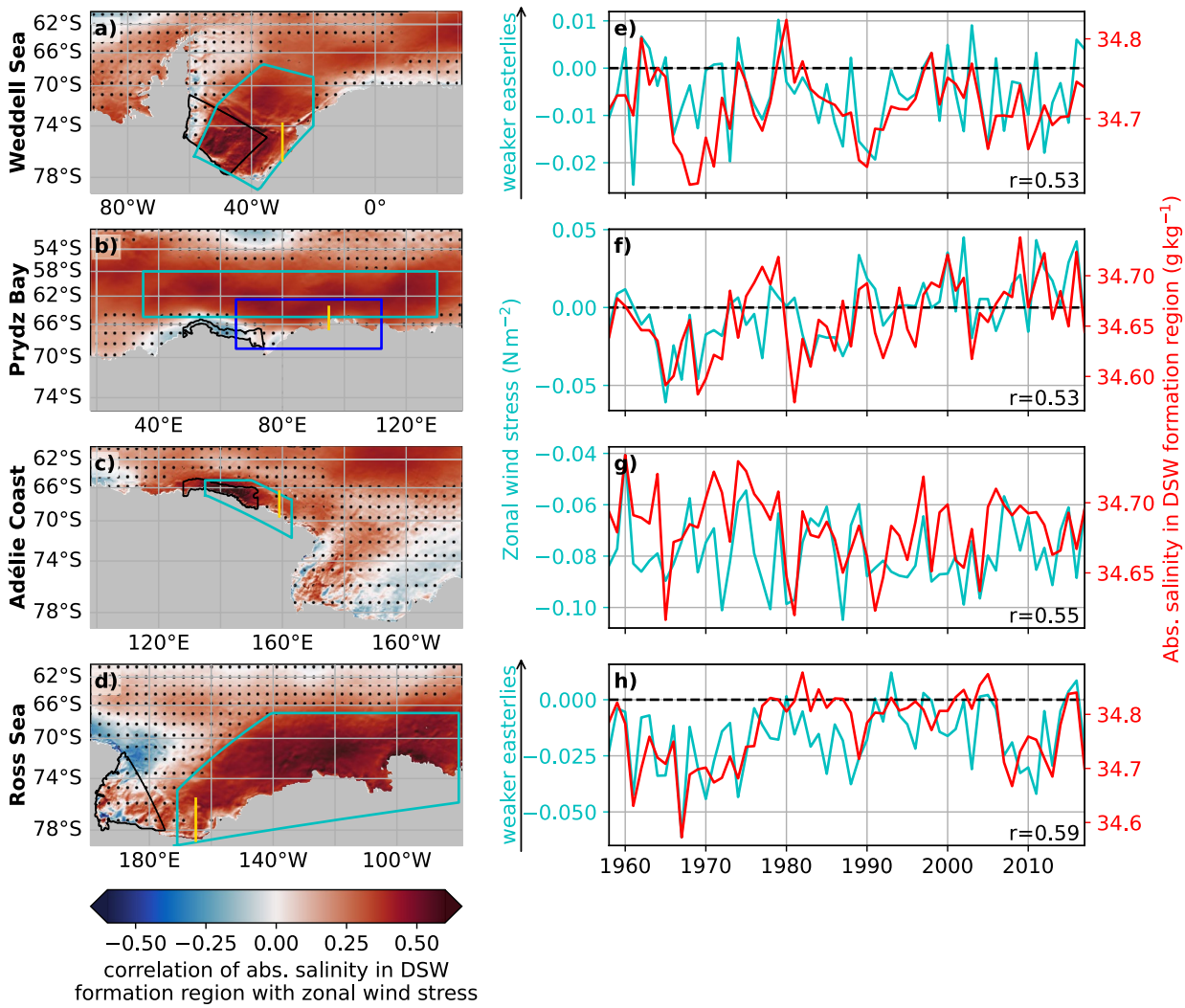

Figure 8. Correlation of the absolute salinity in the Dense Shelf Water (DSW) formation region and the zonal wind stress in the (a, e) Weddell Sea, (b, f) Prydz Bay, (c, g) Adélie Coast, and (d, h) Ross Sea. The maps in (a–d) show the correlation between the salinity averaged in the DSW formation region (black contour) in the upper 300 m between August and October and the zonal wind stress at each grid point. Areas without hatching are significant with $p < 0.05$. (e–h) Time series of the zonal wind stress (cyan lines) averaged over the cyan box in (a–d) and salinity (red lines) in the DSW formation region (outlined in black in a–d). The zonal wind stress was calculated by averaging over months preceding the SWMT which are January–June in the Weddell and Ross Seas (a, d, e, h), January–February in Prydz Bay (b, f), and April–September for the Adélie Coast (c, g). The yellow meridional sections shown are those used to calculate the sea ice transport into the DSW formation region, and the additional blue box in (b) is used to average the wind stress when correlating with the sea ice transport.

Table 3
Correlation Coefficients Between the Salinity in the Dense Shelf Water Formation Region at 0–300 m for August to October and the Zonal Wind Stress, Sea Ice Transport, and Area of Open Water

	Zonal wind stress		Sea ice transport		Area of open water	
Region	*r*	Months	*r*	Months	*r*	Months
Weddell Se	0.53	January–June	−0.37	January–June	0.49	April–June
Prydz Bay	0.53	January–February	(−0.31)	January–June	0.48	August–October
Adélie Coast	0.55	April–September	−0.47	April–September	0.56	July–September
Ross Sea	0.59	January–June	−0.45	January–June	0.60	April–June

Note. All correlations shown are significant at the 99% confidence level, except the one correlation shown in parentheses where the confidence level is 95%. The months used to calculate the temporal mean are given for each variable. Time series of sea ice transport and the area of open water are shown in Supporting Information S1.

correlation indicates that weaker easterlies (i.e., more positive zonal winds) result in a decreased sea ice transport into the DSW formation region. This relationship is most pronounced in the Ross Sea ($r = -0.59$, $p < 0.01$), but significant in all other regions as well (Weddell Sea: $r = -0.49$, Prydz Bay: $r = -0.43$, Adélie Coast: $r = -0.45$, with $p < 0.01$). The sea ice transport from upstream is thus one factor influencing the sea ice coverage in the DSW formation region in autumn and early winter.

To analyze the role of sea ice coverage, the area of open water is averaged over autumn (April–June) for the Weddell and Ross Seas and over the 3 months centered at the peak of the SWMT for Prydz Bay (August–October) and the Adélie Coast (July–September) and correlated with the salinity in the DSW region. The two different periods were chosen due to different seasonal cycles in sea ice concentrations, and to correspond with the time periods of highest correlations. The area of open water is defined as the area where sea ice concentration is 0% within the region used to calculate the SWMT (i.e., black contours in Figure 2). If the area of open water in autumn and/or winter is larger, the salinity in the DSW formation region is often increased (correlations between 0.49 and 0.60 depending on the region, Table 3 and Figure S2 in Supporting Information S1), emphasizing the importance of sea ice conditions on the formation of DSW.

In the Ross Sea, the salinity is additionally influenced by the advection of salt by ocean currents on the shelf. The salinity in the DSW formation region is significantly higher if the salinity advected between the coast and the 1,000-m isobath across 165°W in the previous summer and autumn (January–June) is increased ($r = 0.57$, $p < 0.01$). A comparable relationship could not be found in the other regions.

5. Summary and Discussion

We analyzed the formation and export of AABW from 1958 to 2018 in a 1/10° global ocean–sea-ice model that has previously been shown to capture DSW and AABW production reasonably realistically. The formation of DSW, the precursor of AABW, is estimated by the SWMT on the Antarctic shelf and the export of AABW is defined as the offshore transport across the 1,000-m isobath downstream of DSW formation regions. The formation of DSW/AABW occurs in the four regions known from observations, that is, the Weddell and Ross Seas, Adélie Coast and Prydz Bay, and the mean AABW export from all four regions combined is 8.6 ± 0.9 Sv, in good agreement with Orsi et al. (1999, 2002). We found that both the SWMT and AABW export exhibit strong interannual to decadal variability, which is not correlated between most formation regions except for the Ross Sea and Adélie Coast, the two formation regions closest together. The annual SWMT, the mean salinity in the upper 300 m (in the region of DSW formation between August and October), and the annual AABW export through to the following winter, are all significantly correlated. In the Weddell and Ross Seas, reservoirs of very saline DSW can accumulate at depth after strong events of SWMT, resulting in higher AABW export for up to a decade even in the absence of further strong SWMT after the initial event. The narrower shelf in East Antarctica leads to a more rapid export of DSW, preventing the accumulation of saline DSW in Prydz Bay and the Adélie Coast on multi-year time scales.

We further find that variability in the formation and export of AABW is driven by zonal wind forcing via its impact on sea ice transport and sea ice coverage (Figure 9). Weaker easterlies, or even a reversal to westerlies upstream of the DSW formation region, coincide with increased salinity in the DSW formation region and higher AABW export. A significant link of the variability in the zonal winds to large scale climate modes is only found for Prydz Bay, where weaker easterlies are related to a positive phase of the Southern Annual Mode. Weaker easterlies upstream of the DSW formation region drive decreased sea ice import into the DSW formation regions in summer to early winter, prior to the peak in SWMT. A reduced sea ice coverage and hence greater likelihood of coastal polynyas then increases the formation of DSW. In addition, the advection by coastal currents on the shelf influences the AABW export in the Ross Sea, with an inflow of high salinity waters linked to a higher AABW export.

Overall, our results agree with the mechanisms proposed for a recovery of AABW formation in the Ross Sea in 2015–2018 (Silvano et al., 2020), wherein anomalously weak zonal winds led to a reduced sea ice import into the Ross Sea, which ultimately resulted in increased salinity and export of AABW. Both meridional winds and surface air temperatures had little effect. In this study, we showed that the mechanisms proposed by Silvano et al. (2020) based on a regional case study in the Ross Sea appear to hold at a circumpolar scale in a 60-year integration of a high resolution ocean–sea-ice model with skillful DSW and AABW formation. The importance

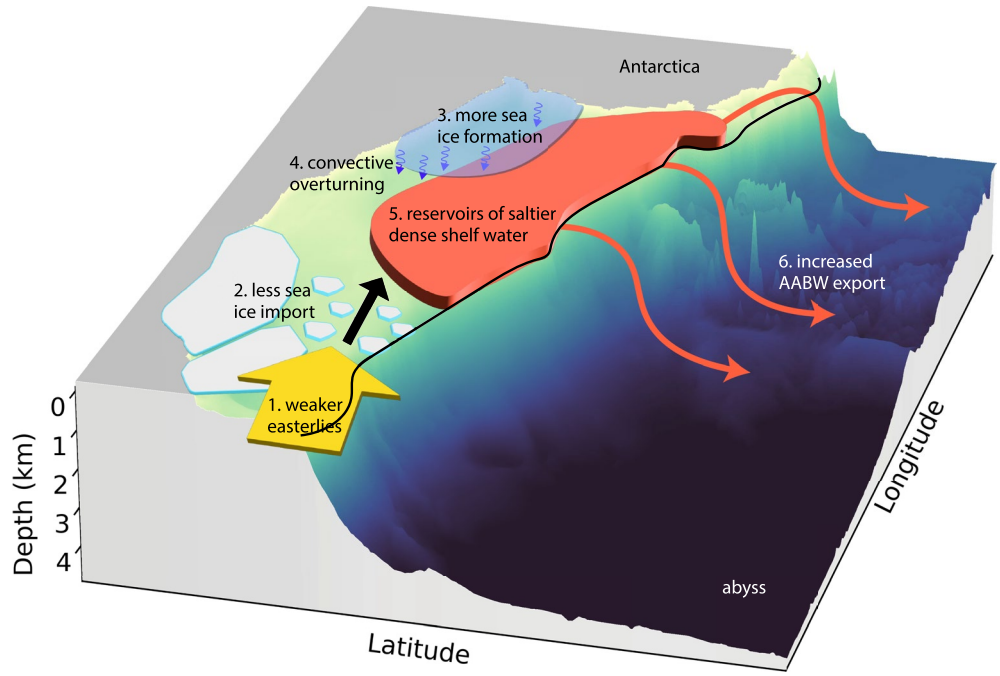

Figure 9. Schematic showing the mechanisms driving increased AABW formation and export. Weaker easterlies (1) over the continental shelf lead to less sea ice import (2) into the formation regions of Dense Shelf Water (DSW). Greater areas of open water in the DSW formation region result in more sea ice formation (3) and more formation of DSW due to brine rejection and convective overturning (4). Reservoirs of saltier DSW form on the shelf (5) which can persist for a few years in the Weddell and Ross Seas where the continental shelf is wide, but flow off the shelf within a few months in Prydz Bay and at the Adélie Coast where the shelf is narrower. An increased export of Antarctic Bottom Water (AABW) is the result (6). An arbitrary bathymetry representing the Antarctic margin is used and the 1,000-m isobath is shown as black line to highlight the shelf break. The mechanisms shown here were also obtained by Silvano et al. (2020) (their Figure 6).

of the inflow on the shelf by coastal currents on the interannual variability of DSW properties was also found in a regional model of the Ross Sea (Assmann & Timmermann, 2005). This is again consistent with our findings.

In contrast to our results, variability in the formation of DSW has been linked to a feedback between the meridional winds and sea ice in the Weddell Sea (McKee et al., 2011; Timmermann, 2002) and Ross Sea (Dinniman et al., 2018). In the Weddell Sea, increased DSW formation is due to enhanced southerly winds, leading to an increased sea ice export out of the DSW formation region. The decreased sea ice concentration results in increased sea ice formation in the following winter and hence more formation of DSW. Although we did not find significant correlations between the meridional wind stress and the formation of DSW for the period of 1958–2018, there is evidence that increased southerlies occur in the Weddell Sea in some years of high DSW formation.

While our estimate of the formation and export of AABW offers unique insight into the variability in all four DSW formation regions during 1958–2018, there are several limitations of the model configuration. First, the data set used to force the model may underestimate katabatic winds (Dong et al., 2020). Second, the model forcing only includes a climatological mean meltwater input. The absence of any interannual variability or long-term trends in glacial meltwater hinders any interpretation of trends in AABW formation in our model simulation. In addition, ACCESS-OM2-01 does not fully resolve the mesoscale on the Antarctic shelf due to a horizontal resolution of 1/10°, and does not include ice shelf cavities. It further lacks tides, which have been shown to have a small impact on AABW export (reduction of ∼10%) in the Weddell Sea (Stewart, 2021), but may be important in the Ross Sea where they have been estimated to change the export by ∼30% (Bowen et al., 2023).

The pronounced interannual variability of AABW formation identified here has potential implications for the interpretation of trends in observational data. In particular, with only infrequent and sparse observations of AABW properties close to Antarctica, sampling at irregular intervals could result in aliasing of DSW and AABW formation rates. Therefore, the interpretation of signals during short time periods could be uncertain if seasonal to interannual variability dominates over long term trends. The recovery of AABW formation

in the Ross Sea in 2015–2018 is for example, only a temporary signal against the backdrop of a long-term freshening trend (Jacobs et al., 2022; Silvano et al., 2020). Both observations with higher spatial and temporal coverage and global climate models which accurately simulate the formation of AABW are required to better understand the mechanisms and effects of a reduction or even shutdown of AABW formation in a warming climate.

Appendix A: Surface Water Mass Transformation Calculation

The surface water mass transformation (SWMT) rate Ω is defined as the volume flux into a particular potential density class σ due to surface buoyancy forcing (Abernathey et al., 2016; Newsom et al., 2016). We discretized the surface density field σ_0 into $\Delta\sigma$ bins of 0.01 kg m^{-3} to compute Ω due to heat fluxes Q and salt fluxes F for each potential density class σ

$$\Omega(\sigma, t) = \frac{1}{\Delta\sigma} \iint_A \left(\frac{\alpha Q}{c_p} + \beta F \right) dA$$

where t is time, A is the outcropping area on the ocean surface between density bins, α is the thermal expansion coefficient, c_p is heat capacity, and β is the haline contraction coefficient. Q includes not only surface heat fluxes but also vertically integrated frazil heat fluxes as they are highly surface intensified. F includes freshwater fluxes (precipitation, evaporation, and run off) multiplied by sea surface salinity, and salt fluxes from sea ice and surface salinity restoring.

Positive values of Ω for a specific density class imply downwelling and therefore formation of Dense Shelf Water (DSW). The mean SWMT rate is sensitive to the choice of the potential density class but the variability is overall robust to this choice (Figure A1), so long as the potential density class is below the peak SWMT. This ensures that an overall density increase in years of more vigorous SWMT where the SWMT peak shifts to a higher density class also results in an increase in our SWMT metric.

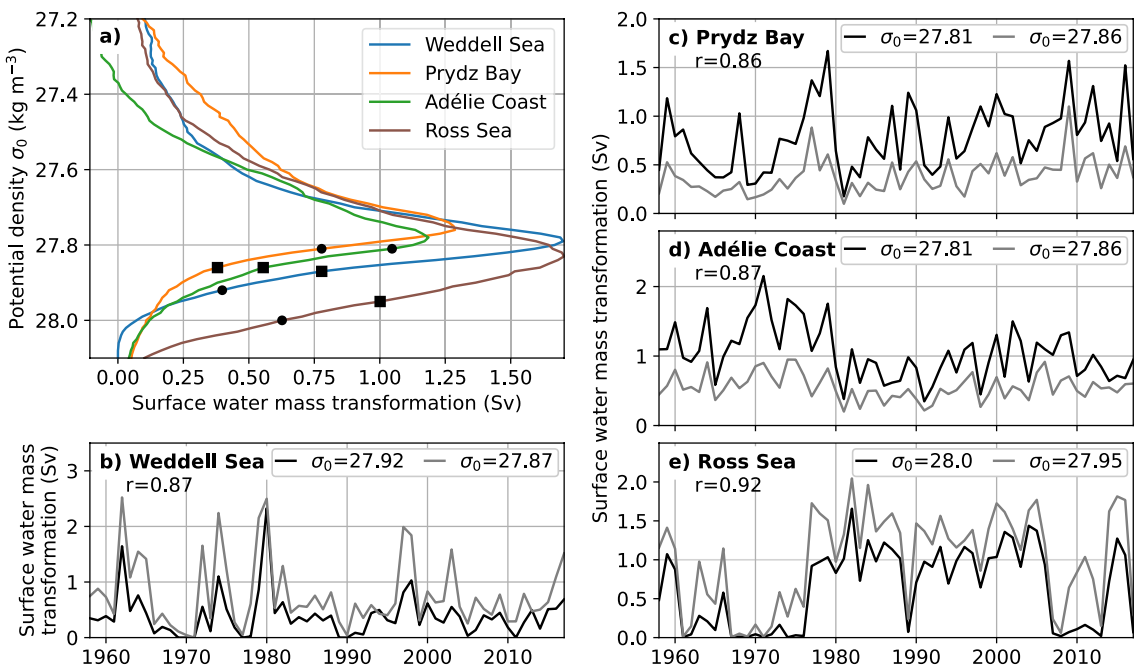

Figure A1. Surface water mass transformation (SWMT) for different potential density classes. (a) SWMT integrated over each of the four regions outlined by the black contours in Figure 2. The circles indicate the potential density class chosen to calculate the rate of SWMT throughout this study. This SWMT is shown as black lines in (b–e), which are identical to the black lines in Figure 5. The gray lines in (b–e) show the SWMT for a different potential density class (0.05 kg m^{-3} lower for the Weddell and Ross Seas and higher for Prydz Bay and the Adélie Coast, indicated by squares in (a)).

The SWMT into potential density classes of DSW is dominated by salt fluxes. They originate mostly from brine rejection during sea ice formation. Therefore, the majority of the SWMT variability can be attributed to sea ice growth in the area where the SWMT occurs each month (orange line in Figure A2 for the Ross Sea). The sea ice growth integrated over the whole region (blue line) used to calculate the SWMT (black contours in Figure 2b) is however not correlated to the SWMT, which emphasizes the importance of localized sea ice growth for the SWMT and hence formation of DSW.

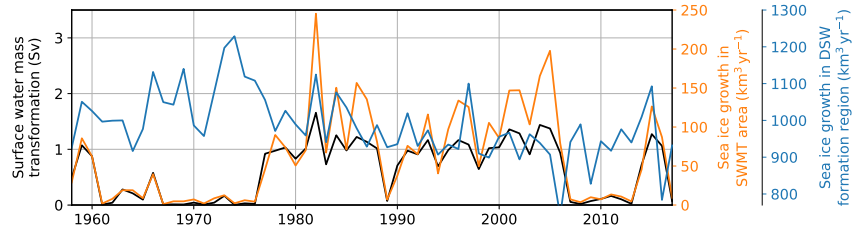

Figure A2. Time series of the surface water mass transformation (SWMT, black line) from Figure 5d and sea ice growth in the Ross Sea. The annual sum of the sea ice growth in the area where the SWMT occurs each month is shown in orange and the sea ice growth integrated over the whole region used to calculate the SWMT (black contours in Figure 2b) is shown in blue.

Data Availability Statement

The model output for the simulations presented in this paper are available in the COSIMA data collection, available from https://doi.org/10.4225/41/5a2dc8543105a. Analysis code is available at https://github.com/schmidt-christina/Schmidt_et_al_2023.

Acknowledgments
This research was undertaken on the National Computational Infrastructure (NCI) in Canberra, Australia, which is supported by the Australian Government. The authors thank the Consortium for Ocean–Sea Ice Modelling in Australia (COSIMA; http://www.cosima.org.au; Project number LP200100406) for making the ACCESS-OM2 suite of models available. AKM was supported by the Australian Research Council (ARC) DECRA Fellowship DE170100184. This research was also supported by the ARC Special Research Initiative, Australian Centre for Excellence in Antarctic Science (Project Number SR200100008) and the ARC Discovery Project DP190100494. We thank two anonymous reviewers for their helpful feedback. Open access publishing facilitated by University of New South Wales, as part of the Wiley - University of New South Wales agreement via the Council of Australian University Librarians.

References

Abernathey, R. P., Cerovecki, I., Holland, P. R., Newsom, E., Mazloff, M., & Talley, L. D. (2016). Water-mass transformation by sea ice in the upper branch of the Southern Ocean overturning. *Nature Geoscience*, *9*(8), 596–601. https://doi.org/10.1038/ngeo2749

Abrahamsen, E. P., Meijers, A. J., Polzin, K. L., Naveira Garabato, A. C., King, B. A., Firing, Y. L., et al. (2019). Stabilization of dense Antarctic water supply to the Atlantic Ocean overturning circulation. *Nature Climate Change*, *9*(10), 742–746. https://doi.org/10.1038/s41558-019-0561-2

Akhoudas, C. H., Sallée, J.-B., Reverdin, G., Meredith, M. P., Naveira-Garabato, A., Haumann, A., et al. (2021). Ventilation of the abyss in the Atlantic sector of the Southern Ocean. *Scientific Reports*, *11*(6760), 6760. https://doi.org/10.1038/s41598-021-86043-2

Assmann, K. M., & Timmermann, R. (2005). Variability of dense water formation in the Ross Sea. *Ocean Dynamics*, *55*(2), 68–87. https://doi.org/10.1007/s10236-004-0106-7

Bowen, M. M., Fernandez, D., Forcen-Vazquez, A., Gordon, A. L., Huber, B., Castagno, P., & Falco, P. (2021). The role of tides in bottom water export from the western Ross Sea. *Scientific Reports*, *11*(1), 1–11. https://doi.org/10.1038/s41598-021-81793-5

Bowen, M. M., Fernandez, D., Gordon, A. L., Huber, B., Castagno, P., Falco, P., et al. (2023). Tides regulate the flow and density of Antarctic Bottom Water from the western Ross Sea. *Scientific Reports*, *13*(1), 3873. https://doi.org/10.1038/s41598-023-31008-w

Carsey, F. D. (1980). Microwave observation of the Weddell Polynya. *Monthly Weather Review*, *108*(12), 2032–2044. https://doi.org/10.1175/1520-0493(1980)108<2032:mootwp>2.0.co;2

Castagno, P., Capozzi, V., DiTullio, G. R., Falco, P., Fusco, G., Rintoul, S. R., et al. (2019). Rebound of shelf water salinity in the Ross Sea. *Nature Communications*, *10*(1), 1–6. https://doi.org/10.1038/s41467-019-13083-8

Depoorter, M. A., Bamber, J. L., Griggs, J. A., Lenaerts, J. T., Ligtenberg, S. R., Van Den Broeke, M. R., & Moholdt, G. (2013). Calving fluxes and basal melt rates of Antarctic ice shelves. *Nature*, *502*(7469), 89–92. https://doi.org/10.1038/nature12567

Dinniman, M. S., Klinck, J. M., Hofmann, E. E., & Smith, W. O. (2018). Effects of projected changes in wind, atmospheric temperature, and freshwater inflow on the Ross Sea. *Journal of Climate*, *31*(4), 1619–1635. https://doi.org/10.1175/JCLI-D-17-0351.1

Dong, X., Wang, Y., Shugui, H. O., Ding, M., Baoling, Y. I., & Zhang, Y. (2020). Robustness of the recent global atmospheric reanalyses for Antarctic near-surface wind speed climatology. *Journal of Climate*, *33*(10), 4027–4043. https://doi.org/10.1175/JCLI-D-19-0648.1

Foppert, A., Rintoul, S. R., Purkey, S. G., Zilberman, N., Kobayashi, T., Sallèe, J. B., et al. (2021). Deep Argo reveals bottom water properties and pathways in the Australian-Antarctic basin. *Journal of Geophysical Research Ocean*, *126*(12), 1–18. https://doi.org/10.1029/2021JC017935

Gordon, A. L. (1966). Potential temperature, oxygen and circulation of bottom water in the Southern Ocean. *Deep Research Oceanographic Abstracts*, *13*(6), 1125–1138. https://doi.org/10.1016/0011-7471(66)90704-2

Gordon, A. L., Huber, B., McKee, D., & Visbeck, M. (2010). A seasonal cycle in the export of bottom water from the Weddell Sea. *Nature Geoscience*, *3*(8), 551–556. https://doi.org/10.1038/ngeo916

Gordon, A. L., Huber, B. A., & Abrahamsen, E. P. (2020). Interannual variability of the outflow of Weddell Sea Bottom Water. *Geophysical Research Letters*, *47*(4), 1–9. https://doi.org/10.1029/2020GL087014

Gordon, A. L., Orsi, A. H., Muench, R., Huber, B. A., Zambianchi, E., & Visbeck, M. (2009). Western Ross Sea continental slope gravity currents. *Deep Sea Research Part II Topical Studies in Oceanography*, *56*(13–14), 796–817. https://doi.org/10.1016/j.dsr2.2008.10.037

Griffies, S. M. (2012). Elements of the Modular Ocean Model (MOM). *GFDL Model Documentation*, *3*(C), 1–631.

Griffies, S. M., Danabasoglu, G., Durack, P. J., Adcroft, A. J., Balaji, V., Böning, C. W., et al. (2016). OMIP contribution to CMIP6: Experimental and diagnostic protocol for the physical component of the Ocean Model Intercomparison Project. *Geoscientific Model Development*, *9*(9), 3231–3296. https://doi.org/10.5194/gmd-9-3231-2016

Haumann, F. A., Gruber, N., Münnich, M., Frenger, I., & Kern, S. (2016). Sea-ice transport driving Southern Ocean salinity and its recent trends. *Nature*, *537*(7618), 89–92. https://doi.org/10.1038/nature19101

Heuzé, C. (2021). Antarctic Bottom Water and North Atlantic Deep Water in CMIP6 models. *Ocean Science*, *17*(1), 59–90. https://doi.org/10.5194/os-17-59-2021

Hosking, J. S., Orr, A., Marshall, G. J., Turner, J., & Phillips, T. (2013). The influence of the Amundsen-Bellingshausen Seas low on the climate of West Antarctica and its representation in coupled climate model simulations. *Journal of Climate*, *26*(17), 6633–6648. https://doi.org/10.1175/JCLI-D-12-00813.1

Hunke, E. C., Lipscomb, W. H., Turner, A. K., Jeffery, N., & Elliot, S. (2015). *CICE: The Los Alamos Sea Ice Model documentation and software user's manual version 5.1 (Technical report)*. Los Alamos National Laboratory.

Jacobs, S. S., Amos, A. F., & Bruchhausen, P. M. (1970). Ross Sea oceanography and Antarctic Bottom Water formation. *Deep Research Oceanography Abstracts*, *17*(6), 935–962. https://doi.org/10.1016/0011-7471(70)90046-X

Jacobs, S. S., Giulivi, C. F., & Dutrieux, P. (2022). Persistent Ross Sea freshening from imbalance West Antarctic ice shelf melting. *Journal of Geophysical Research Ocean*, *127*(3), e2021JC017808. https://doi.org/10.1029/2021jc017808

Johnson, G. C. (2008). Quantifying Antarctic Bottom Water and North Atlantic Deep Water volumes. *Journal of Geophysical Research Ocean*, *113*(5), 1–13. https://doi.org/10.1029/2007JC004477

Jullion, L., Garabato, A. C., Meredith, M. P., Holland, P. R., Courtois, P., & King, B. A. (2013). Decadal freshening of the Antarctic Bottom Water exported from the Weddell Sea. *Journal of Climate*, *26*(20), 8111–8125. https://doi.org/10.1175/JCLI-D-12-00765.1

Jullion, L., Naveira Garabato, A. C., Bacon, S., Meredith, M. P., Brown, P. J., Torres-Veldes, S., et al. (2014). The contribution of the Weddell Gyre to the lower limb of the Global Overturning Circulation. *Journal of Geophysical Research Ocean*, *119*(6), 3357–3377. https://doi.org/10.1002/2013JC009725

Kiss, A. E., Hogg, A. M., Hannah, N., Boeira Dias, F., Brassington, G. B., Chamberlain, M. A., et al. (2020). ACCESS-OM2 v1.0: A global ocean–sea ice model at three resolutions. *Geoscientific Model Development*, *13*(2), 401–442. https://doi.org/10.5194/gmd-13-401-2020

Kobayashi, T. (2018). Rapid volume reduction in Antarctic Bottom Water off the Adélie/George V Land coast observed by deep floats. *Deep Sea Research Part II Topical Studies in Oceanography*, *140*(July), 95–117. https://doi.org/10.1016/j.dsr.2018.07.014

Lago, V., & England, M. H. (2019). Projected slowdown of Antarctic Bottom Water formation in response to amplified meltwater contributions. *Journal of Climate*, *32*(19), 6319–6335. https://doi.org/10.1175/JCLI-D-18-0622.1

Li, Q., England, M. H., Hogg, A. M., Rintoul, S. R., & Morrison, A. K. (2023). Abyssal ocean overturning slowdown and warming driven by Antarctic meltwater. *Nature*, *615*(7954), 841–847. https://doi.org/10.1038/s41586-023-05762-w

Lumpkin, R., & Speer, K. (2007). Global ocean meridional overturning. *Journal of Physical Oceanography*, *37*(10), 2550–2562. https://doi.org/10.1175/JPO3130.1

Marshall, G. J. (2003). Trends in the Southern Annular Mode from observations and reanalyses. *Journal of Climate*, *16*(24), 4134–4143. https://doi.org/10.1175/1520-0442(2003)016(4134:TITSAM)2.0.CO;2

McKee, D. C., Yuan, X., Gordon, A. L., Huber, B. A., & Dong, Z. (2011). Climate impact on interannual variability of Weddell Sea Bottom Water. *Journal of Geophysical Research Ocean*, *116*(5), 1–17. https://doi.org/10.1029/2010JC006484

Mensah, V., Nakayama, Y., Fujii, M., Nogi, Y., & Ohshima, K. I. (2021). Dense water downslope flow and AABW production in a numerical model: Sensitivity to horizontal and vertical resolution in the region off Cape Darnley polynya. *Ocean Modelling*, *165*, 101843. https://doi.org/10.1016/j.ocemod.2021.101843

Meredith, M. P., Watson, A. J., Van Scoy, K. A., & Haine, T. W. (2001). Chlorofluorocarbon-derived formation rates of the deep and bottom waters of the Weddell Sea. *Journal of Geophysical Research Ocean*, *106*(C2), 2899–2919. https://doi.org/10.1029/2000jc900119

Moorman, R., Morrison, A. K., & Hogg, A. M. C. (2020). Thermal responses to Antarctic ice shelf melt in an eddy-rich global ocean-sea ice model. *Journal of Climate*, *33*(15), 6599–6620. https://doi.org/10.1175/JCLI-D-19-0846.1

Morrison, A. K., McCHogg, A., England, M. H., & Spence, P. (2020). Warm Circumpolar Deep Water transport toward Antarctica driven by local dense water export in canyons. *Science Advances*, *6*(18), 1–10. https://doi.org/10.1126/sciadv.aav2516

Naveira Garabato, A. C., McDonagh, E. L., Stevens, D. P., Heywood, K. J., & Sanders, R. J. (2002). On the export of Antarctic Bottom Water from the Weddell Sea. *Deep Sea Research Part II Topical Studies in Oceanography*, *49*(21), 4715–4742. https://doi.org/10.1016/S0967-0645(02)00156-X

Naveira Garabato, A. C., Williams, A. P., & Bacon, S. (2014). The three-dimensional overturning circulation of the Southern Ocean during the WOCE era. *Progress in Oceanography*, *120*, 41–78. https://doi.org/10.1016/j.pocean.2013.07.018

Naveira Garabato, A. C., Zika, J. D., Jullion, L., Brown, P. J., Holland, P. R., Meredith, M. P., & Bacon, S. (2016). The thermodynamic balance of the Weddell Gyre. *Geophysical Research Letters*, *43*(1), 317–325. https://doi.org/10.1002/2015GL066658

Newsom, E. R., Bitz, C. M., Bryan, F. O., Abernathey, R., & Gent, P. R. (2016). Southern Ocean deep circulation and heat uptake in a high-resolution climate model. *Journal of Climate*, *29*(7), 2597–2619. https://doi.org/10.1175/JCLI-D-15-0513.1

Ohshima, K. I., Fukamachi, Y., Williams, G. D., Nihashi, S., Roquet, F., Kitade, Y., et al. (2013). Antarctic Bottom Water production by intense sea-ice formation in the Cape Darnley polynya. *Nature Geoscience*, *6*(3), 235–240. https://doi.org/10.1038/ngeo1738

Orsi, A. H., Johnson, G. C., & Bullister, J. L. (1999). Circulation, mixing, and production of Antarctic Bottom Water. *Progress in Oceanography*, *43*(1), 55–109. https://doi.org/10.1016/S0079-6611(99)00004-X

Orsi, A. H., Smethie, W. M., & Bullister, J. L. (2002). On the total input of Antarctic waters to the deep ocean: A preliminary estimate from chlorofluorocarbon measurements. *Journal of Geophysical Research Ocean*, *107*(8), 3122. https://doi.org/10.1029/2001jc000976

Patara, L., & Böning, C. (2014). Abyssal ocean warming around Antarctica strengthens the Atlantic overturning circulation. *Geophysical Research Letters*, *41*(11), 3972–3978. https://doi.org/10.1002/2014GL059923

Pellichero, V., Sallée, J. B., Chapman, C. C., & Downes, S. M. (2018). The southern ocean meridional overturning in the sea-ice sector is driven by freshwater fluxes. *Nature Communications*, *9*(1), 1–9. https://doi.org/10.1038/s41467-018-04101-2

Purich, A., & England, M. H. (2021). Historical and future projected warming of Antarctic Shelf Bottom Water in CMIP6 models. *Geophysical Research Letters*, *48*(10), 1–15. https://doi.org/10.1029/2021GL092752

Purkey, S. G., & Johnson, G. C. (2013). Antarctic Bottom Water warming and freshening: Contributions to sea level rise, ocean freshwater budgets, and global heat gain. *Journal of Climate*, *26*(16), 6105–6122. https://doi.org/10.1175/JCLI-D-12-00834.1

Purkey, S. G., Smethie, W. M., Gebbie, G., Gordon, A. L., Sonnerup, R. E., Warner, M. J., & Bullister, J. L. (2018). A synoptic view of the ventilation and circulation of Antarctic Bottom Water from chlorofluorocarbons and natural tracers. *Annual Review of Marine Science*, *10*(1), 503–527. https://doi.org/10.1146/annurev-marine-121916-063414

Sarmiento, J. L., Gruber, N., Brzezinski, M. A., & Dunne, J. P. (2004). High-latitude controls of thermocline nutrients and low latitude biological productivity. *Nature*, *427*(6969), 56–60. https://doi.org/10.1038/nature02127

Sen Gupta, A., & England, M. H. (2004). Evaluation of interior circulation in a high-resolution global ocean model. Part I: Deep and bottom waters. *Journal of Physical Oceanography*, *34*(12), 2592–2614. https://doi.org/10.1175/JPO2651.1

Silvano, A., Foppert, A., Rintoul, S. R., Holland, P. R., Tamura, T., Kimura, N., et al. (2020). Recent recovery of Antarctic Bottom Water formation in the Ross Sea driven by climate anomalies. *Nature Geoscience*, *13*(12), 780–786. https://doi.org/10.1038/s41561-020-00655-3

Solodoch, A., Stewart, A. L., Hogg, A. M., Morrison, A. K., Kiss, A. E., Thompson, A. F., et al. (2022). How does Antarctic Bottom Water cross the Southern Ocean? *Geophysical Research Letters*, *49*(7), 1–11. https://doi.org/10.1029/2021gl097211

Spence, P., Griffies, S. M., England, M., McCHogg, A., Saenko, O. A., & Jourdain, N. C. (2014). Rapid subsurface warming and circulation changes of Antarctic coastal waters by poleward shifting winds. *Geophysical Research Letters*, *41*(1), 4601–4610. https://doi.org/10.1002/2014GL060613

Spence, P., Holmes, R. M., Hogg, A. M. C., Griffies, S. M., Stewart, K. D., & England, M. H. (2017). Localized rapid warming of West Antarctic subsurface waters by remote winds. *Nature Climate Change*, *7*(8), 595–603. https://doi.org/10.1038/NCLIMATE3335

Stewart, A. L. (2021). Mesoscale, tidal, and seasonal/interannual drivers of the Weddell Sea overturning circulation. *Journal of Physical Oceanography*, *51*(12), 3695–3722. https://doi.org/10.1175/jpo-d-20-0320.1

Swart, S., Johnson, K., Mazloff, M. R., Meijers, A., Meredith, M. P., Newman, L., & Sallée, J.-B. (2018). Return of the Maud Rise polynya: Climate litmus or sea ice anomaly? *Bulletin of the American Meteorological Society*, *99*(8), S185–S190.

Talley, L. D. (2013). Closure of the global overturning circulation through the Indian, Pacific, and Southern Oceans: Schematics and transports. *Oceanography*, *26*(1), 80–97. https://doi.org/10.5670/oceanog.2013.07

Timmermann, R. (2002). Simulations of ice-ocean dynamics in the Weddell Sea 2. Interannual variability 1985–1993. *Journal of Geophysical Research*, *107*(C3), 3025. https://doi.org/10.1029/2000jc000742

Tsujino, H., Urakawa, S., Nakano, H., Small, R. J., Kim, W. M., Yeager, S. G., et al. (2018). JRA-55 based surface dataset for driving ocean–sea-ice models (JRA55-do). *Ocean Modelling*, *130*(December 2017), 79–139. https://doi.org/10.1016/j.ocemod.2018.07.002

Turner, J., Phillips, T., Hosking, J. S., Marshall, G. J., & Orr, A. (2013). The Amundsen Sea Low. *International Journal of Climatology*, *33*(7), 1818–1829. https://doi.org/10.1002/joc.3558

Whitworth, I., & Orsi, A. H. (2006). Antarctic Bottom Water production and export by tides in the Ross Sea. *Geophysical Research Letters*, *33*(12), 1–4. https://doi.org/10.1029/2006GL026357

Williams, G. D., Bindoff, N. L., Marsland, S. J., & Rintoul, S. R. (2008). Formation and export of dense shelf water from the Adélie depression, East Antarctica. *Journal of Geophysical Research Ocean*, *113*(4), 1–12. https://doi.org/10.1029/2007JC004346